

The effect of polyindole-based binder-free coating on the corrosion behavior of mild steel in 3.5% NaCl solution

Rukan SUNA KARATEKİN (✉ rukansuna@mersin.edu.tr)

Özlem KILIÇ

Sedef KAPLAN

Meltem KAHYA DÜDÜKCÜ

Research Article

Keywords: corrosion, polyindole, organic inhibitor, Electrochemical impedance spectroscopy

Posted Date: April 27th, 2023

DOI: <https://doi.org/10.21203/rs.3.rs-2858099/v1>

License:   This work is licensed under a Creative Commons Attribution 4.0 International License.

[Read Full License](#)

Additional Declarations: No competing interests reported.

Version of Record: A version of this preprint was published at Journal of Applied Electrochemistry on August 18th, 2023. See the published version at <https://doi.org/10.1007/s10800-023-01965-1>.

Abstract

The influence of three polyindole samples on the corrosion rate of mild steel (MS) in absence and presence of different amounts of acetonitrile was investigated in 1 M HClO₄. All samples were characterized by Scanning Electron Microscopy (SEM), Energy Dispersive X-ray Spectroscopy (EDX), Fourier-transform infrared spectroscopy (FTIR), UV-vis spectroscopy, X-ray Powder Diffraction (XRD), and contact angle measurements. Through measurements, it was determined that the polymers differ from each other on the basis of morphology, conjugation, molecular mass, and crystallinity. Also, it was found that all samples include FeCl₃ used as an oxidant. Among the samples, PIn1 has the highest anti-corrosive property as it includes the highest amount of Fe and the highest density of hydrophobic group such as ClO₄⁻. According to the results, it was found that PIn1 inhibited the cathodic corrosion reaction of MS in 3.5% NaCl and showed 98% protection efficiency.

1. Introduction

Corrosion is a major problem in the industrial field due to its impact on safety, economy, and the environment [1]. Many scientific studies are carried out on the protection of metals and alloys from corrosion. Most of organic compounds containing nitrogen, sulfur, oxygen atoms or/and multiple bonds are effective inhibitors for corrosion of many metals and alloys. Conductive polymers are widely used as organic coatings for corrosion protection due to their low toxic effects, environmental stability, and electrical conductivity [2–5]. The conductive polymer adsorbed on the metal surface acts as a barrier preventing aggressive ions from reaching the metal surface [3].

In recent years polyindole and its derivatives have been used commonly to protect corrosion of stainless and mild steel because of good thermal stability, high redox property and slow degradation rate when compared to polyaniline and polypyrrole [6]. However, short-term protection and weak adhesion strength are major limitations of polyindole in the the corrosion protection area usage [7]. To date polyindole has been electrochemically deposited on different materials and its corrosion inhibition performance has been investigated [8,9]. To overcome the mentioned limitations, polyindole was deposited on the material with different synthesise routes or different monomers. For example, Ramirez et al synthesized Poly (indole-5-carboxylic acid), Poly (indole-6-carboxylic acid) and Poly (indole-7-carboxylic acid) electrochemically on stainless steel. All polymers were examined for their corrosion protection at different temperatures in acidic solution. They emphasized that position of –COOH group in polymer structure affects the hydrophobicity, and this influences the anticorrosive protection of AISI304 stainless steel [7]. Several researchers reported that they prepared composites containing polyindole, carbon-based materials and binder agent deposited on the work surface. For example, Nayak et al., used the carboxy functionalized MWCNT/PIn nanohybrid dispersed in the epoxy matrix to enhance its anti-corrosion and barrier properties on mild (MS) steel in 3.5 wt. % NaCl solution [10]. Mobin et al. investigated the corrosion inhibition performance of graphene-polyindole composite synthesized on low carbon steel in 3.5% NaCl solution. Researchers used both curing agent and epoxy resin when fabricating working electrode [6]. In

mentioned studies, either polyindole was deposited on metal electrochemically or stabilized thanks to a curing agent and/or epoxy resin.

In this study, polyindole was chemically synthesized in electrolytes containing 1 M HClO₄ and different molar ratios of HClO₄-acetonitrile and bonded on mild steel without binder, stabilizer, and supporting material. The anti-corrosion performance of polyindole on mild steel was examined in an aqueous medium containing 3.5 wt % NaCl by using electrochemical impedance spectroscopy (EIS), open circuit potential (E_{OCP}), and potentiodynamic polarization curves. In addition, the effects of temperature and immersion times on the corrosion protection ability of polyindole, which has the highest anti-corrosive properties, were investigated.

2. Materials and Methods

Synthesis of polyindole series

To synthesize polyindole, three different electrolyte media were used as follows;

- 1 M HClO₄ (1)
- 1:4 ratio of acetonitrile and 1 M HClO₄ (2)
- 1:1 ratio of acetonitrile and 1 M HClO₄ (3)

Initially, 16 mM indole was dissolved in each media mentioned above via ultrasonication and 1.2 gr FeCl₃ was added into monomer solutions. The solution was mixed 24 h to obtain brown polyindole suspension. After these steps, suspension was centrifuged and polymer washed several times with bidistilled water.

Note: Each media was labeled with a number as shown above, and these labels also indicate the name of the polyindoles. For example, PIn1 refers to indole which is oxidized in electrolyte number 1.

Characterizations of polyindoles

The structural characterization was performed by an FT-IR spectrometer JASCO-6800, in the range of 450-4000 cm⁻¹. Uv-vis spectrums were recorded via in the 200–700 nm range, using Shimadzu 1700 spectrophotometer. All samples were dissolved in methanol to perform the measurement. For morphological analysis, a scanning electron microscope Zeiss (Supra 55) SEM instrument was used.

Preparation of working electrodes

A mild steel rod embedded in a polyester block with an exposed area of 0.09 cm² was used as a working electrode. To obtain the ink form of PIn1, PIn2, and PIn3, a certain amount of each polyindole was dissolved in 1 mL methanol and sonicated for 20 minutes. Then, 100µL polymer ink was dropped into mild steel, and the electrode was dried at 50 °C.

Corrosion tests

The corrosion tests of PIn1, PIn2, and PIn3 catalysts were carried out in 3.5% NaCl solution using CHI-660C electrochemical workstation. A Pt mesh (2 cm² surface area) as the counter electrode, Ag/AgCl electrode as the reference and mild steel as the working electrode were used. The working electrode, the mild steel plate (SS), has a chemical composition (wt%) of: 0.08 C, 0.16 Si, 0.028 S, 0.019 Cr, 0.43 Mn, 0.014 Ni, 0.041 Cu, 0.0016 Mo, 0.041 V, 0.0033 Sn, 0.0006 Co, 0.0018 Ti, 0.015 Nb, 0.0033 Al and 99.13 Fe. Before corrosion tests, the working electrode was dipped in 3.5% NaCl solution and OCP was continuously observed until steady-state potential was obtained. The EIS measurements were performed at OCP within the frequency range of 10⁻² to 10⁵ Hz in 3.5 % NaCl solution by applying 0.005 V voltage amplitude. Polarization curves were recorded at both anodic and cathodic region with a constant sweep rate of 1 mVs⁻¹. Before the beginning of the experiments, the mild steel was polished with a series of wet sandings (200, 600, and 1200) of different grit sizes. After polishing the electrode, it was washed with bidistilled water and dried at room temperature.

3. Result and Discussion

SEM and EDX result

Figure 1 displays SEM images of PIn1, PIn2, and PIn3 at different magnifications. It was observed that all samples morphology are different from each other because of using different electrolyte media. With increasing acetonitrile volume in electrolyte, the polymers (PIn2 and PIn3) grew with compact morphology. While the morphology of PIn1 and PIn2 is almost similar, PIn1 has smaller particles. It is seen from the SEM images recorded at high magnifications that PIn1 has a porous structure compared to the others. Comparing EDX result (Figure 2) of three samples, it was found that only PIn1 includes Fe element belongs to the FeCl₃. The Cl element intensity increase with the amount of HClO₄ in the electrolyte that the polymer is grown in.

XRD measurement

The XRD diffrogram of PIn1, PIn2 and PIn3 is shown in Figure 3. As can be seen from the figure, in the range of 2θ=15°-30°, all samples have a broad peak indicating the typical polymer response [11]. While PIn1 and PIn2 have sharp peaks at 2θ=21° and 22° showing crystallinity of both samples, PIn3 has a sharp peak at 2θ=19° with weak intensity. This result shows that PIn1 and PIn2 predominantly exhibit crystalline structures compared to PIn3. The sharp peak at 2θ = 30.74° seen in the XRD pattern belongs to the Fe(Cl)₃. It was concluded that FeCl₃, which is used as an oxidant agent to obtain polymers, participates in the entire polymer chain according to XRD. Additionally, while the EDX result shows only PIn1 includes Fe atom, the XRD result shows that three samples have Fe content. PIn2 and PIn3 are thought to have too low Fe content to be detected by EDX.

UV-vis measurement

The Uv-vis spectrum of PIn1, PIn2 and, PIn3 in the range of 235-800 nm are shown in Figure 4. The absorption bands observed in the first region (235-300 nm) belongs to the π - π^* , and the band position different for each polymer. Additionally, the peak at 575 nm indicating polaronic transitions shifted to lower wavelength for polymers that grew in the monomer media containing acetonitrile [12].

While no band was observed for PIn1 at 700 nm, a broad peak appeared for polymers grown in acetonitrile and perchloric acid. It was observed that the intensity of the mentioned band increased for the polymer obtained from the solution with high acetonitrile content. From these results, it is concluded that polymers conjugations and molecular mass of samples differ from each other.

FTIR measurement

In the FTIR spectrum (Figure5) a strong peak observed at approximately 730 cm^{-1} for all samples indicates out-of-plane bending of the C-H bond of the benzene ring in indole moiety. The peaks seen at 3300 cm^{-1} belongs to N-H stretching vibration which confirmed the presence of polyindole. Also, the bands appeared at 1570 cm^{-1} indicates the N-H bond is still present implying nitrogen presence in indole is not in the polymerization site. Furthermore, the peaks observed at 1450 cm^{-1} and 1610 cm^{-1} are due to the stretching mode of the benzene ring of polyindole. The other common peak observed in all spectra at 1040 cm^{-1} belongs to the preferred perchlorate anion as solvent. These results are compatible with earlier studies [13]. The mentioned peak intensity is highest for PIn1 because it is growing in a higher volume of HClO_4 solvent. This result shows that PIn1 contains the ClO_4^- anion, which is stated to be the hydrophobic group, more intensely [14]. In addition, out of the three samples, only the PIn3 sample contains -OH bonds of adsorbed H_2O . This shows that the PIn3 sample has a hydrophilic surface.

Contact angle measurements

The wettability test is an essential measurement to further investigate the anticorrosive properties of coating samples. The strong hydrophobic property of the sample is one of the reasons for the protection of metal from the corrosive species. The higher contact angle value indicates strong hydrophobic properties of the sample. The contact angle values were given in Figure 6. Therefore, PIn has the strongest hydrophobic property among coating samples because it contains hydrophobic groups in polymer chains.

OCP and EIS measurement:

Figure 7 shows the Eocp-t diagram of PIn1/MS, PIn2/MS, PIn3/MS and bare MS in 3.5 wt % NaCl at room temperature. In the presence of polyindole the potential shifted to positive value in the comparison to bare MS. Among the electrodes which are coated with polyindole, PIn1 has the maximum positive shift indicating shows maximum protecting for corrosion species. PIn1 exhibited higher barrier effect as a result of the formation of more adherent and uniform coating on MS.

After E_{OCP} measurements, EIS measurements were performed in 3.5 wt% NaCl at room temperature to gain further insight on corrosion resistances of PIn1/MS, PIn2/MS, PIn3/MS and bare MS electrodes. Figure 8 shows the Nyquist diagrams obtained at the steady state potential of all electrodes. All diagrams were fitted via Zview 2b and the proposed equivalent circuits (EC) are shown in Figure 8b. Nyquist diagrams of PIn2, PIn3 and bare MS electrodes simulated with EC1 include electrolyte (R_e) and charge transfer resistances (R_{ct}). PIn2 diagram includes R_e , R_p (pore resistance), and R_{ct} in accordance with EC2. The increase in R_e is thought to be due to the hydrophobic property of polyindole coated on the mild steel surface. Among coated electrodes, PIn1 has the highest R_e value and it was observed that this value increased with the content of $HClO_4$. Additionally, the R_{ct} value of blank MS, PIn1, PIn2 and PIn3 is 1081, 8231, 4649, and 2116 ohm, respectively (Table 1). The $\log z$ - $\log f_{req}$ and phase angle- $\log f_{req}$ diagrams are also shown in Fig 8a. It can be seen from both diagrams that PIn1 has the highest resistance and negative value phase angle compared to the others. Therefore, it can be said, the PIn1 electrode shows the highest anti-corrosive properties.

Table1. The electrochemical impedance parameters obtained by fitting EIS equivalent circuit for PIn1, PIn2, PIn3 and bare MS in 3.5 wt. % NaCl solution

Electrode	R_e (Ω)	R_p (Ω)	CPE_{1-T} (μF)	CPE_{1-P}	R_{CT} (Ω)	CPE_{2-T} (μF)	CPE_{2-P}
PIn1	116.5	1899	9.25	0.740	8231	99.8	0.714

Electrode	$R_e(\Omega)$	$R_1(\Omega)$	CPE_{1-T} (F)	CPE_{1-P}
Bare MS	9.72	1081	40.4×10^{-4}	0.661
PIn3	21.87	2116	1.6×10^{-4}	0.615
PIn2	73.27	4649	2.25×10^{-4}	0.374

Polarization curves measurement of all electrodes

The polarization curves were used to evaluate protective performance of PIn1/MS, PIn2/MS and PIn3/MS. In general, the lower current corrosion density means higher anti corrosive properties of coatings. Figure 9 and 10 show the cathodic and anodic polarization curves of bare MS PIn1/MS, PIn2/MS and PIn3/MS, respectively. In both polarization curves, it was observed that these three coatings have anti corrosive properties. PIn1 showed the highest protective performance with the lowest current corrosion density. In Table 2, the polarization curves parameters such as E_{corr} , cathodic Tafel slope, corrosion current (I_{corr}), polarization resistance (R_p), and protection efficiency ($\% \eta$) are given, respectively. As can be seen in Table 2 and in Table 3, in both regions E_{corr} shifted to positive potentials while polarization resistance increased following the order PIn1>PIn2>PIn3. PIn1 exhibited the highest

protection performance with 98 % protection efficiency in the cathodic region and 83.29 % in the anodic region.

Table 2. Cathodic polarization curve parameters for Bare MS, PIn1/MS, PIn2/MS and PIn3/MS in 3.5 wt% NaCl solution.

Sample	E _{corr} (mV)	I _{corr} ($\mu\text{A}/\text{cm}^2$)	R _p (ohm/cm ²)	bc (mV/decade)	% η
Bare MS	-0.619	142	254.9	342.7	
PIn1/MS	-0.47	2.8	5073	229,6	98
PIn2/MS	-0.604	53.2	676	385	62.5
PIn3/MS	-0.58	12	2226	222.7	91.54

Table 3. Anodic polarization curve parameters for Bare MS, PIn1/MS, PIn2/MS and PIn3/MS in 3.5 wt.% NaCl solution

Sample	E _{cor} (mV)	I _{corr} ($\mu\text{A}/\text{cm}^2$)	R _p (ohm/cm ²)	bc (mv/decade)	% η
Bare MS	-0.737	18.8	724	267.95	
PIn1/MS	-0.544	3.14	9659	136.76	83.29
PIn2/MS	-0.618	5.85	4574	157.65	68.8
PIn3/MS	-0.722	16.3	1288.8	176.89	13.29

By all measurements, PIn1 exhibited the highest anti-corrosive property. So, for further investigation of its protective performance, EIS diagrams at 25 °C on different days and polarization curves were recorded at different temperatures (10, 20, 30, 40 and, 50 °C).

Long-term corrosion inhibition performance of PIn1:

Before EIS measurement, E_{OCP}-time diagram was recorded as shown in Figure 11. E_{OCP} values shifted to negative values due to the corrosion products formed on the surface with the increase in immersion time [15]. Figure 12 shows Nyquist and Bode plots obtained for PIn1 sample after 1d, 2d, 3d, 4d, 7d, 8d, 9d and 10 d immersion times.

The Nyquist diagrams of PIn1 (Figure 12) consist of capacitive loops represented by suppressed semicircles on all days. Electrochemical impedance parameters derived from EIS fitting curves for PIn1 in

3.5 wt% NaCl solution and at different immersion times are given in Table 4. For day 0, the Nyquist plot has two resistances including pore resistance (R_p) and charge transfer resistance (R_{ct}), while the Nyquist plot for other days has a new resistance (R_{cs}) in the middle-frequency region related to corrosion species. The total corrosion resistance, commonly referred to as polarization resistance, is the sum of R_{cs} and R_{ct} , and these values increased with immersion time. Moreover, in the low frequencies, with immersion times phase angle increased towards a negative value, and resistance got higher.

CPE2 and CPE3 are constant phase elements of the film of corrosion products and the electrical double layer between the coating layer and the substrate, respectively [16]. It is observed that CPE3 increases with immersion times, indicating the penetration of the corrosion to the coating sample increased [17]. After 9 days, decreasing R_{ct} indicates the protection of the coatings becomes weakened, and the corrosion medium reached the substrate surface [18].

Table 4. Electrochemical impedance parameters derived from EIS fitting curves for Pln1 in 3.5 wt% NaCl solution and at different immersion times.

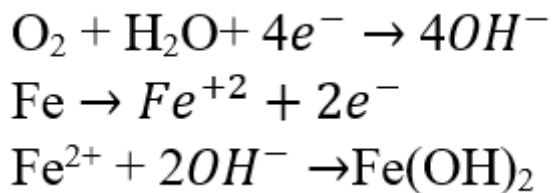
Immersion time (day)	$R_p(\Omega)$	$CPE_{1-T}(\mu F)$	CPE_{1-P}	$R_{Cc}(\Omega)$	$CPE_{2T}(\mu F)$	CPE_{2-P}	$R_{ct}(\Omega)$	$CPE_{3-T}(\mu F)$	CPE_{3-P}
0	1899	9.25	0.740				8231	99.8	0.714
1	432.5	0.0227	0.85	3966	28.2	0.55	11296	28	0.92
2	752.5	0.223	0.64	6723	21.6	0.56	15932	31.6	0.95
3	958	0.0086	0.71	10020	21.9	0.54	18906	39	0.97
4	1398	0.215	0.63	12209	18.2	0.55	24756	42	0.972
7	2046	0.109	0.68	17341	17.1	0.52	32838	66.6	0.971
8	2401	0.00898	0.7	22629	16.7	0.51	35957	78.6	0.97
9	3246	0.00654	0.72	37683	17.5	0.47	37274	100	1.019
10	2762	0.00903	0.69	35565	16.5	0.5	32293	128	1.01

Characterization of Pln1 after its corrosion test

After corrosion measurement, Pln1 was peel of the surface and used for its characterization measurement. In Figure 13, SEM images with different magnifications of Pln1 before and after immersion in aggressive medium are shown. Looking at the high magnifications image, the morphology of Pln1 includes new layers with the brighter region after corrosion measurement. This is a typical observation for SEM measurement when the sample includes metal or metal compound particles. At low magnifications, it was observed that porous surface of Pln1 turned into a compact surface with passive layer formation. From EDX measurement (Figure 14) it can be clearly seen that, Fe content increase after corrosion tests. The high amount of Fe is thought to be due to steel and polymer containing $FeCl_3$.

Before and after corrosion measurement, PIn1's FTIR spectrums are shown in Figure 15. After corrosion measurement new peaks of Fe-OH based on corrosion species stretching appeared at 1010 cm^{-1} and 900 cm^{-1} [19]. Comparing Figure 15a and Figure 15b, it was observed that the peaks location and intensities changed. This result may be due to the interaction between the functional group in PIn1 and corrosion species. In addition,

In Figure 16, XRD diffrograms of the PIn1 sample before and after long-term corrosion tests in NaCl solution are given. When looking at the peeled samples, diffrogram includes $\alpha\text{-FeOOH}$ and Fe(OH)_3 . The two Fe-based compounds are products of the corrosion process. The possible mechanism suggested is as follow:



In the presence of oxygen and water, Fe(OH)_2 easily converted to Fe(OH)_3 . In fact, another possible reaction can take place between FeCl_3 which adsorbed to PIn1 and OH^- to produce Fe(OH)_3 . It has been reported that $\gamma\text{-FeOOH}$ forms rapidly in a neutral solution and transforms into the stable $\alpha\text{-FeOOH}$ form due to its unstable properties [20].

Effect of temperature

The corrosion inhibition performance of PIn1 in 3.5% NaCl solution at different temperatures (10, 20, 30, 40, and, 50 °C) was investigated with cathodic polarization curves. (Fig 17). It was determined that E_{ocp} shifted to active direction, I_{corr} increased and R_{por} decreased with increasing temperature (Table 5). From these results, it was concluded that corrosion reaction rate increased with temperature. The reason is that with temperature the adhesive properties of PIn1 may have decreased and corrosion species penetrated the substrate. To further investigation temperature effect on protective properties of PIn1, EIS measurement was performed. Nyquist plots of PIn1 which are recorded at different temperatures are shown in Figure 18. All plots include semicircles in the low-frequency region belongs to charge transfer resistance. The diameter of the semicircles is equal to R_{ct} , and it was observed that it decreases with the increase in temperature. Both measurements show that the anticorrosive property of PIn1 decreases with increasing temperature.

Table 5. Cathodic polarization curves data of PIn1 at 10, 20, 30, 40, and 50 °C

Temperature (°C)	E _{cor} (V)	I _{corr} (μA/cm ²)	R _p (ohm/cm ²)	b _c (mV/decade)
Bare	-0.619	142	254.9	342.7
10	-0.548	2.204	18185	198.2
20	-0.601	5.534	7616	248.3
30	-0.606	8.350	5933	213.76
40	-0.631	14.07	3146	291.29
50	-0.637	41.4	1017.8	296.8

Conclusion

- Polyindoles were successfully synthesized in both HClO₄ and a mixed electrolyte containing HClO₄ and acetonitrile. Polymers that were ink form (PIn1, PIn2 and PIn3) applied to mild steel were stored without binder and epoxy.
- Although all samples were based on polyindole, UV-vis, FTIR, SEM, XRD measurements showed that they differed from each other on the basis of morphology, conjugation, molecular mass and crystallinity.
- OCP diagrams recorded for all samples showed that polymers growing in solution with high amounts of perchloric acid exhibit stable and nobler E_{ocp} value. Among samples, the highest anti-corrosive property with the noblest E_{ocp} belongs to the PIn1 which was grown in only HClO₄ electrolyte.
- According to the polarization curves measurement, PIn1 inhibited the cathodic corrosion reaction of MS in 3.5% NaCl and protection efficiency is found to be 98%
- The EIS result shows that the PIn1 coating reduces the corrosion rate of mild steel for nine days.
- It was observed that the anti-corrosion property of PIn1 decreased with increasing temperature due to the weakening of its adhesive property.
- To introduce the corrosion mechanism and anti-corrosive property of PIn1, the sample characterization was performed before and after corrosion tests. It was understood that the coating sample includes Fe(OH)₃ and α-FeOOH after immersion in NaCl. These two products are thought to originate from mild steel (in the form of Fe) and polymer (including FeCl₃)

Declarations

Funding

Not applicable

Data availability

All data generated or analyzed during this study are included in this published article

Conflict of interest

The authors declare no competing interests.

Contributions

R.S.Karatekin: Supervision, Writing – review & editing.; **M.Düdükcü** Investigation, Conceptualization, **Özlem KILIÇ:** Software, Methodology, Data curation, original draft preparation, **S.Kaplan:** Investigation, Conceptualization, Software, Methodology,

Compliance with Ethical Standards

Not applicable

References

1. Shahryari Z, Gheisari K, Yeganeh M, Ramezanzadeh B, “Corrosion mitigation ability of differently synthesized polypyrrole (PPy-FeCl₃ & PPy-APS) conductive polymers modified with Na₂MoO₄ on mild steel in 3.5% NaCl solution: Comparative study and optimization.” *Corros. Sci.*, 193 109894 (2021)
2. Düdükcü M, Avci G, “Electrochemical synthesis and corrosion inhibition performance of poly-5-aminoindole on stainless steel.” *Prog. Org. Coatings*, 97 110–114 (2016)
3. Duran B, “Potentiodynamic synthesis of poly(N-vinyl carbazole) films on stainless steel to enhance corrosion resistance in sulfuric acid solution.” *Polym. Technol. Mater.*, 61 1833–1843 (2022)
4. Al Jabri H, Devi MG, Al-Shukaili MA, “Development of polyaniline – TiO₂ nano composite films and its application in corrosion inhibition of oil pipelines.” *J. Indian Chem. Soc.*, 100 100826 (2023)
5. Abdul Rahman F, Basirun WJ, Johan MR, Ghazali N, “Corrosion inhibition of particulate and tubular polyaniline in polyvinyl butyral for mild steel protection.” *Mater. Lett.*, 336 133898 (2023)
6. Mobin M, Ansar F, Shoeb M, Parveen M, Aslam J, “Synergistic effect of graphene polyindole nanocomposite for enhanced corrosion protection of aqueous coating in 3.5% NaCl solution for low carbon steel.” *Nano Sel.*, 2 293–302 (2021)
7. Ramírez AMR, Mieres F, Pineda F, Grez P, Heyser C, “Electrosynthesis of polyindole-carboxylic acids on stainless steel and their corrosion protection at different temperatures in acidic solution.” *Prog. Org. Coatings.*, 172 107075 (2022)
8. Düdükcü M, Köleli F, “Electrochemical synthesis of polyindole on 304-stainless steel in LiClO₄-acetonitrile solution and its corrosion performance.” *Prog. Org. Coatings*, 55 324–329 (2006)

9. Tüken T, Yazici B, Erbil M, "The use of polyindole for prevention of copper corrosion." *Surf. Coatings Technol.*, 200 4802–4809 (2006)
10. Nayak SR, Mohana KNS, Hegde MB, Rajitha K, Madhusudhana AM, Naik SR, "Functionalized multi-walled carbon nanotube/polyindole incorporated epoxy: An effective anti-corrosion coating material for mild steel." *J. Alloys Compd.*, 856 (2021)
11. Barkoula NM, Alcock B, Cabrera NO, Peijs T, "Flame-Retardancy Properties of Intumescent Ammonium Poly(Phosphate) and Mineral Filler Magnesium Hydroxide in Combination with Graphene." *Polym. Polym. Compos.*, 16 101–113 (2008)
12. Mozaffari S, Behdani J, Ghorashi SMB, "Synthesis of polyindole nanoparticles and its copolymers via emulsion polymerization for the application as counter electrode for dye-sensitized solar cells." *Polym. Bull.*, 79 6777–6796 (2022)
13. Aşkin T, Suna Karatekin R, Dündükcü M, "Synthesis and characterization of highly conductive poly(indole-4-aminoquinaldine) copolymer." *J. Mater. Sci. Mater. Electron*, 33 17923–17938 (2022)
14. Xu B, Zhai Y, Zhu Y, Peng C, Wang T, Zhang C, Li C, Zeng G, "The adsorption mechanisms of ClO₄⁻ onto highly graphited and hydrophobic porous carbonaceous materials from biomass." *RSC Adv.*, 6 93975–93984 (2016)
15. Zhang G, Jiang E, Wu L, Ma W, Yang H, Tang A, Pan F, "Corrosion protection properties of different inhibitors containing PEO/LDHs composite coating on magnesium alloy AZ31." *Sci. Rep.*, 11 1–14 (2021).
16. [16] Hiromoto S, Doi K, "Effect of polyethylene glycol modification on the corrosion behavior of hydroxyapatite-coated AZ31 Mg alloy under tensile deformation." *Corros. Sci.*, 212 110931 (2023)
17. Peng C, Cao G, Gu T, Wang C, Wang Z, Sun C, "The effect of dry/wet ratios on the corrosion process of the 6061 Al alloy in simulated Nansha marine atmosphere." *Corros. Sci.*, 210 110840 (2023)
18. Zhang J, Zhu Q, Wang Z, Wang X, Yan J, "Flake-like ZnAl alloy powder modified waterborne epoxy coatings with enhanced corrosion resistance, *Prog. Org.*" *Coatings.*, 175 107367 (2023)
19. Wang HL, Cui JY, Jiang WF, "Synthesis, characterization and flocculation activity of novel Fe(OH)₃-polyacrylamide hybrid polymer." *Mater. Chem. Phys.*, 130 993–999 (2011)
20. He CG, Song ZB, Gan YZ, Ye RW, Zhu RZ, Liu JH, Xu ZB, "Study on the Corrosion Behavior and Mechanism of ER8 Wheel Steel in Neutral NaCl Solution." *Coatings.*, 12 (2022)

Figures

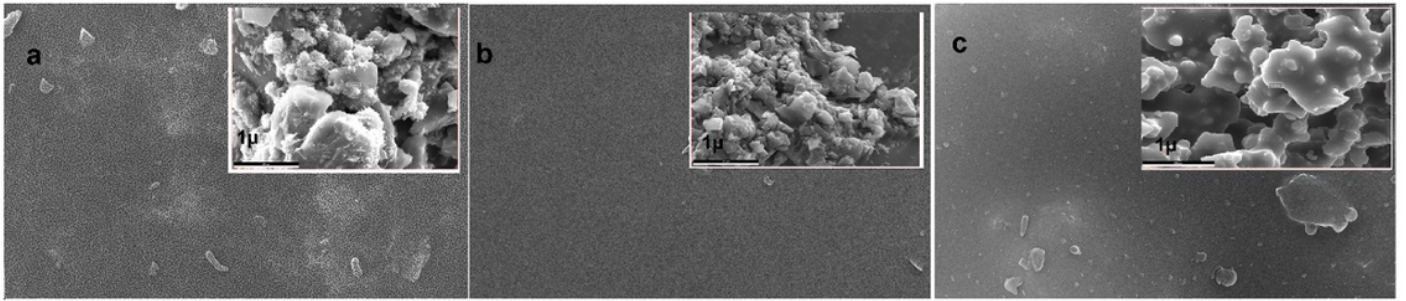


Fig. 1

Figure 1

SEM images a) PIn1 b) PIn2 and, PIn3 at different magnifications.

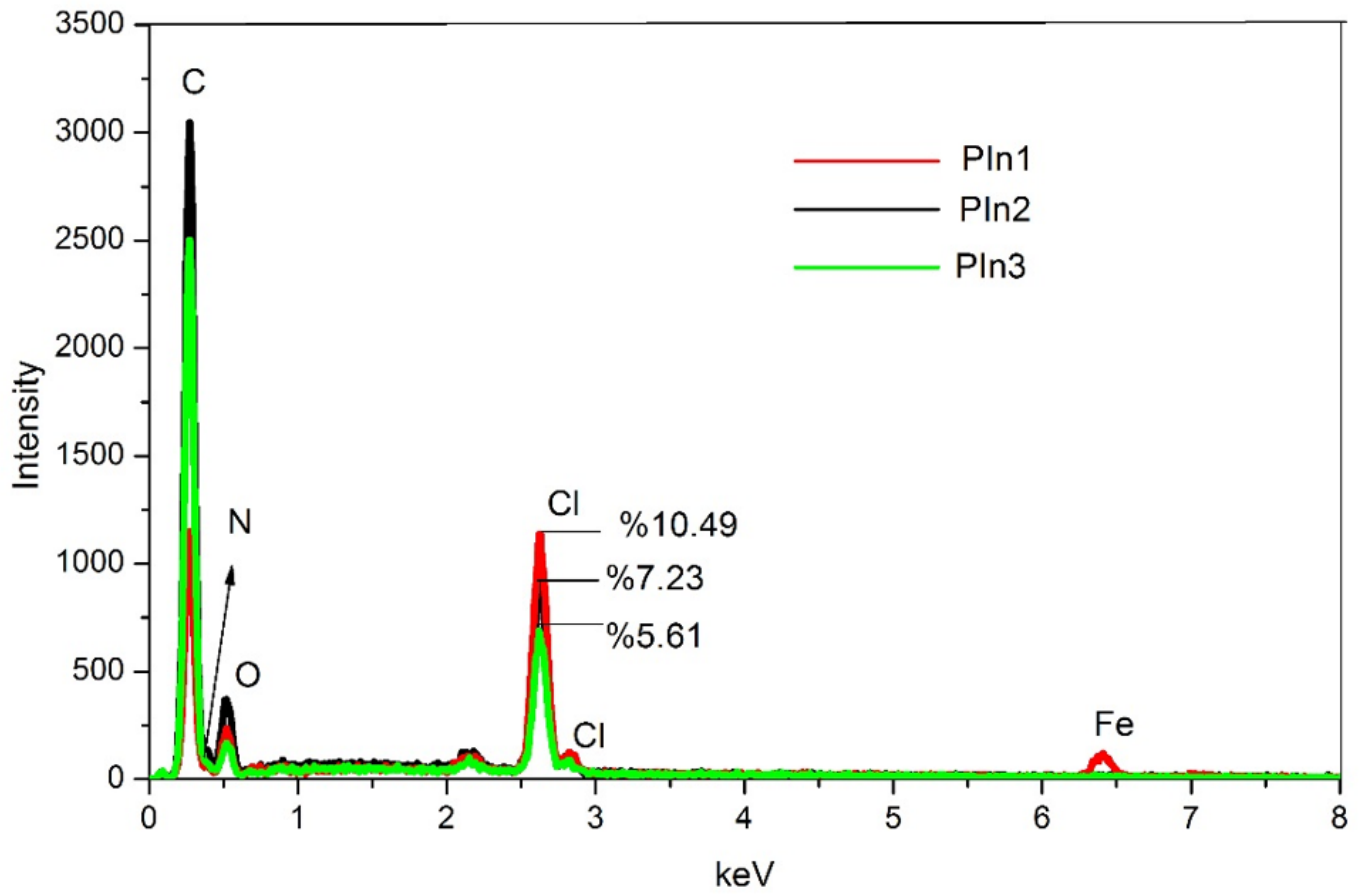


Fig 2.

Figure 2

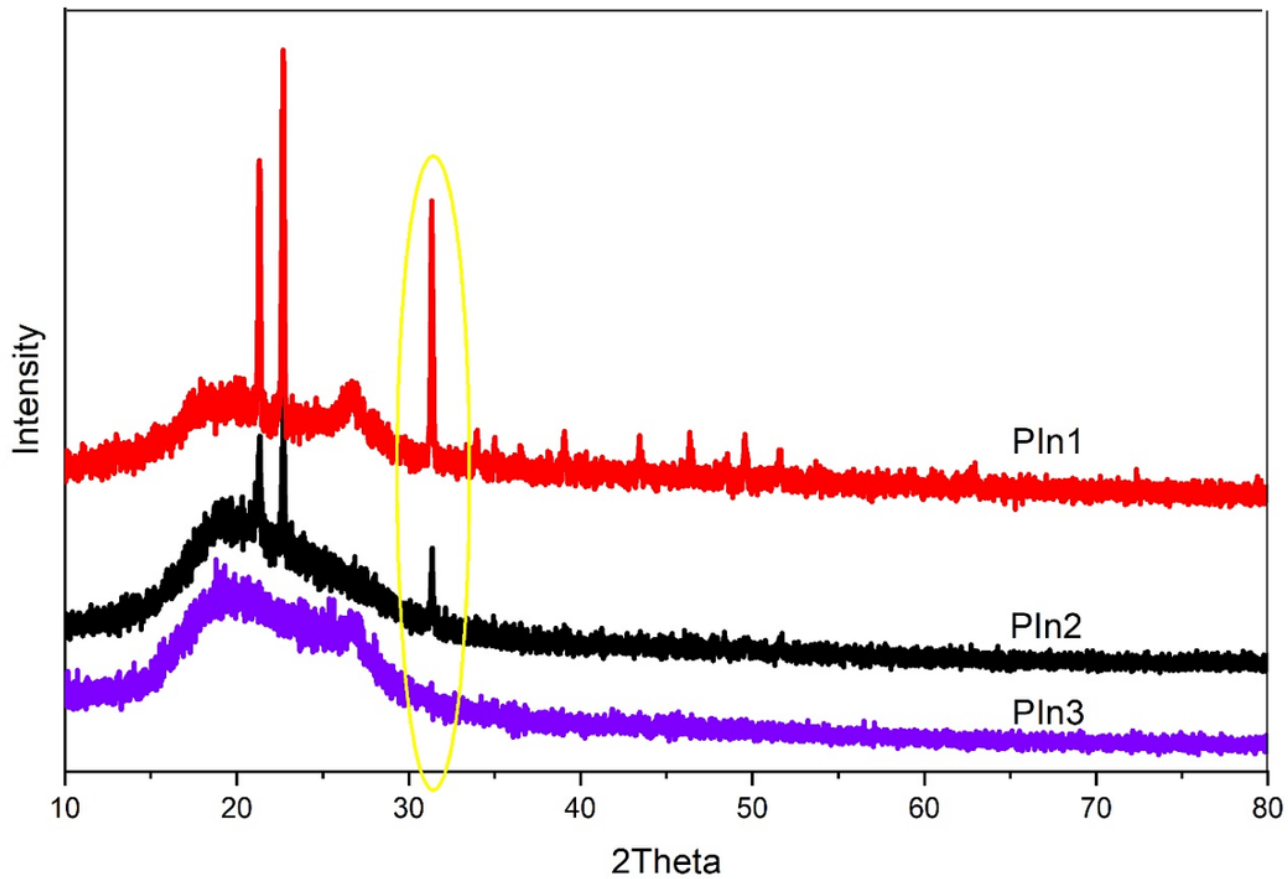


Fig 3.

Figure 3

XRD patterns of PIn1, PIn2 and PIn3

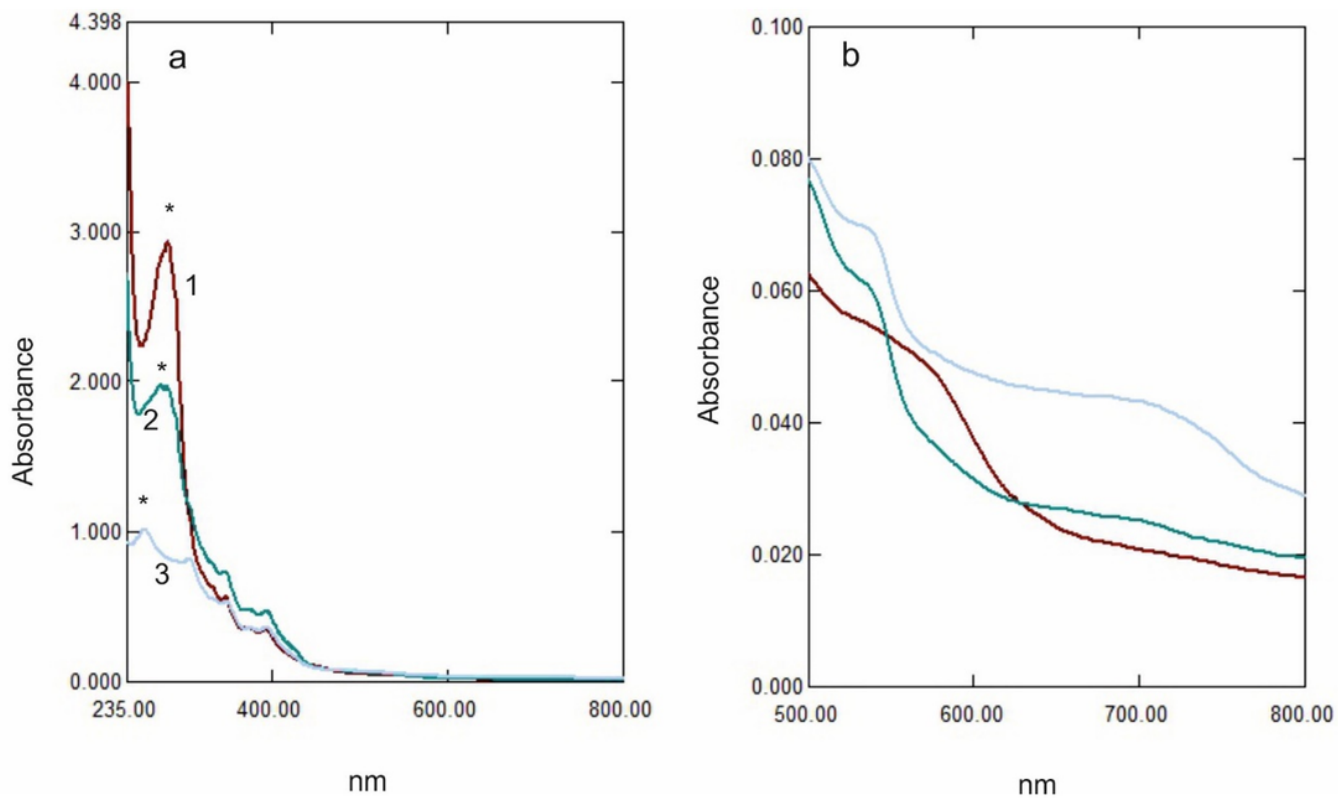


Fig 4.

Figure 4

UV-vis spectrum of 1) PIn1, 2) PIn2 and, 3) PIn3 a) in the range of 235-800 nm b) in the range of 500-800 nm

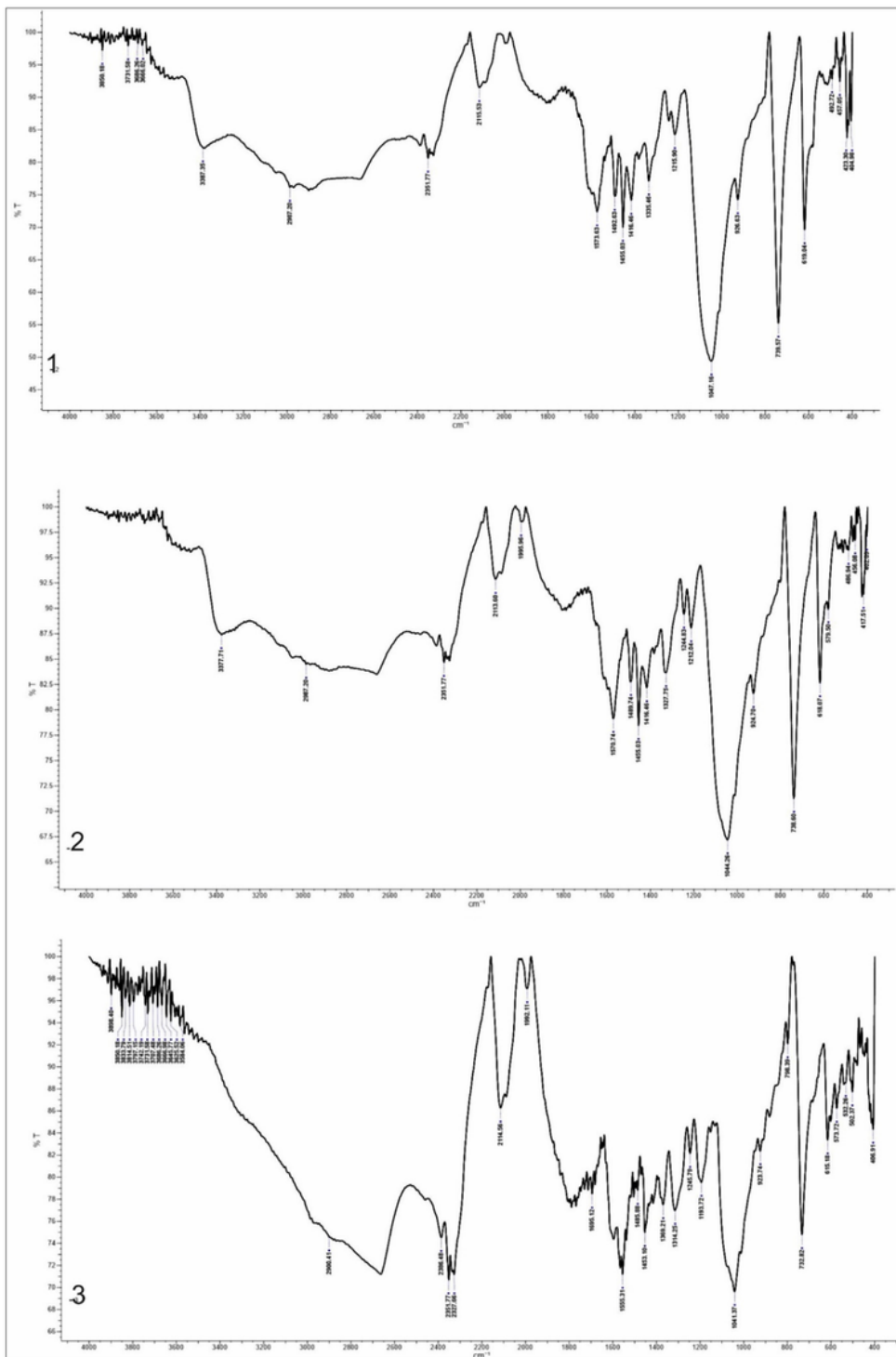


Fig 5.

Figure 5

FTIR spectrum of 1) Pln1, 2)Pln2 and, 3)Pln3

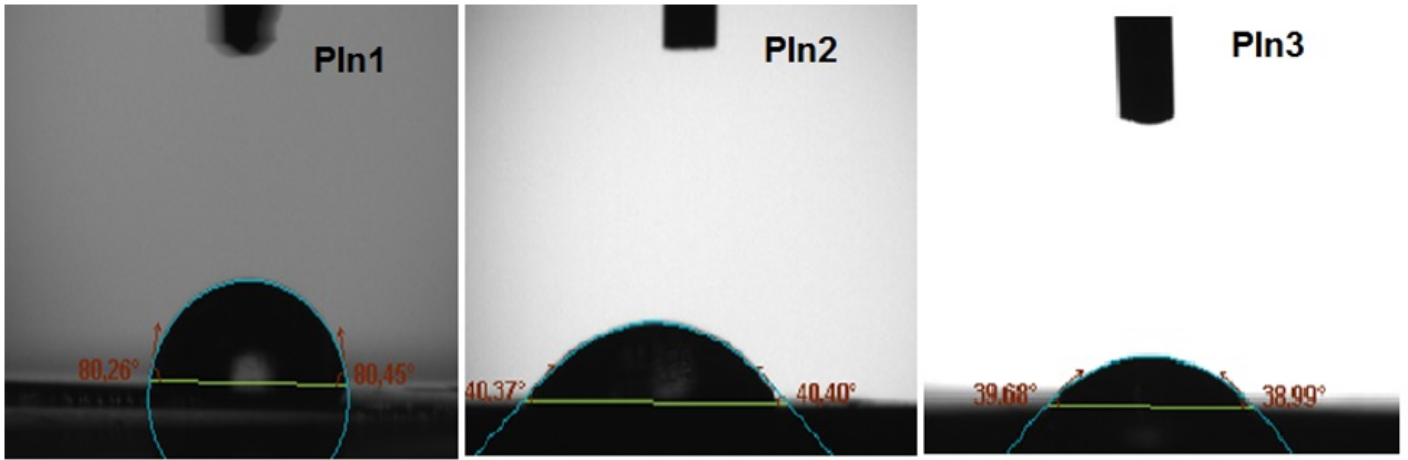


Fig. 6.

Figure 6

Contact *angle* measurement of PIn1, PIn2, and PIn3.

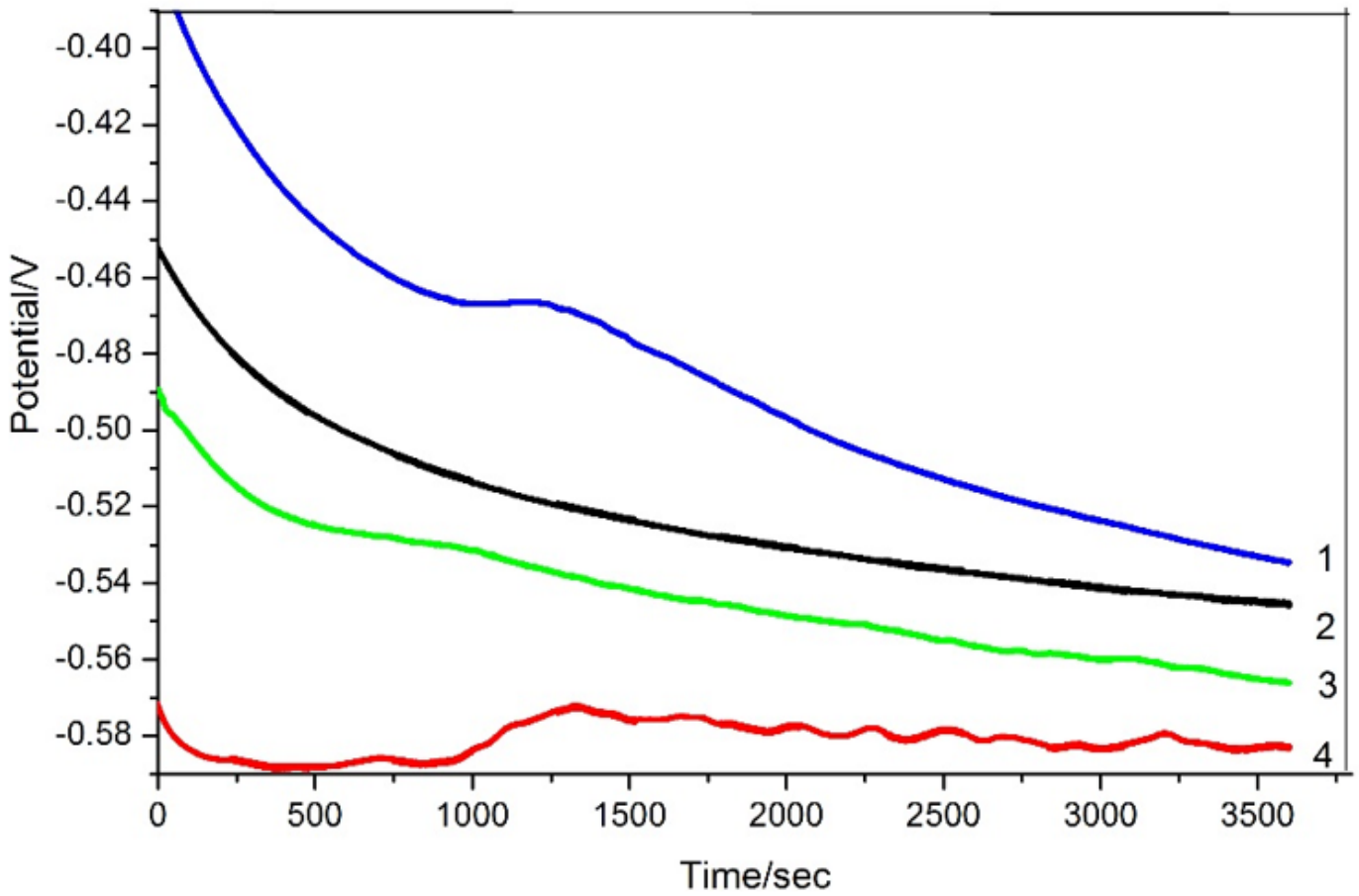


Fig 7.

Figure 7

Eocp-time diagram of 1) Pln1/MS, 2)Pln2/MS 3)Pln3/MS and 4)Bare MS

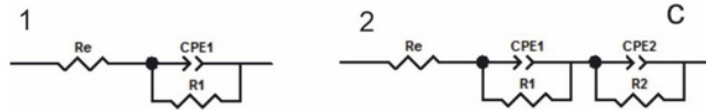
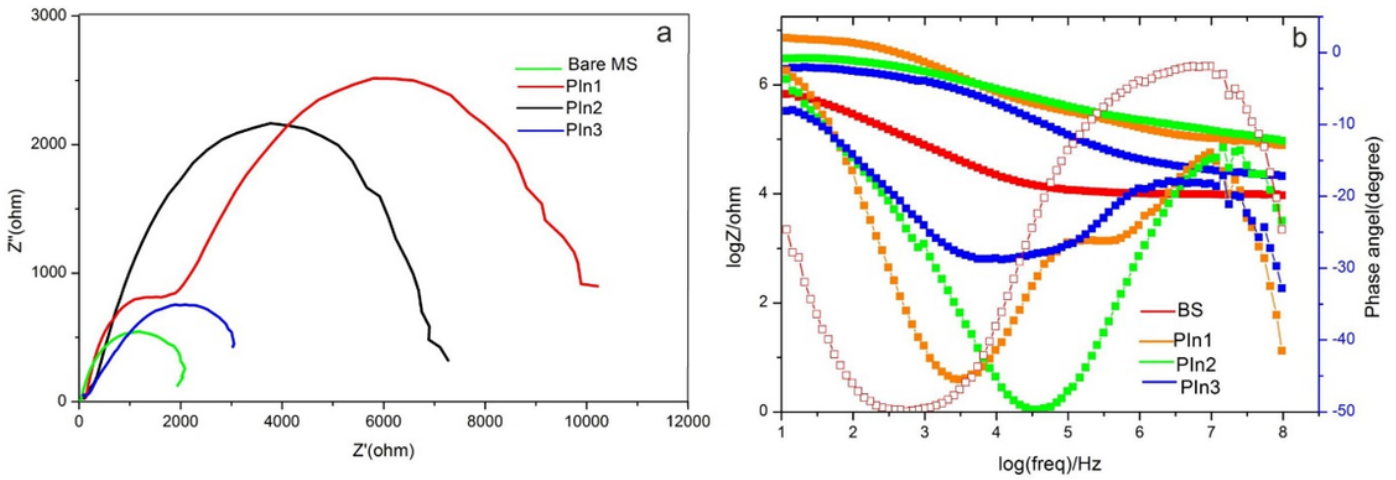


Fig 8

Figure 8

a)Nyquist plot, b) Bode and phase angel plot of Pln1/MS Pln2/MS,Pln3/MS and bare MS c) Equivelant circuit for of Pln1/MS Pln2/MS,Pln3/MS and bare MS

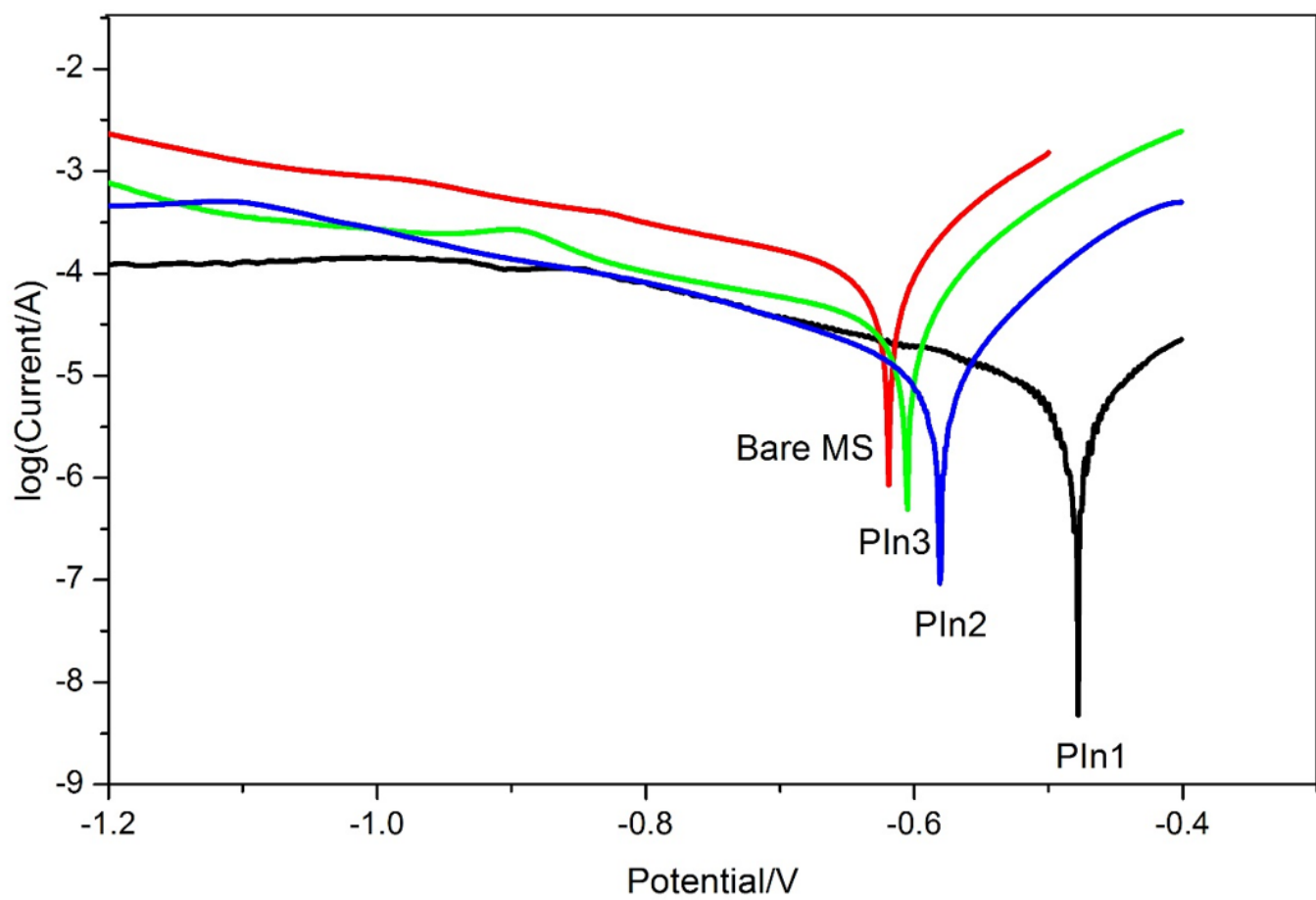


Fig 9.

Figure 9

Cathodic polarizatn curves of Bare MS, PIn1/MS, PIn2/MS and PIn3/MS in 3.5 % NaCl at 20 °C

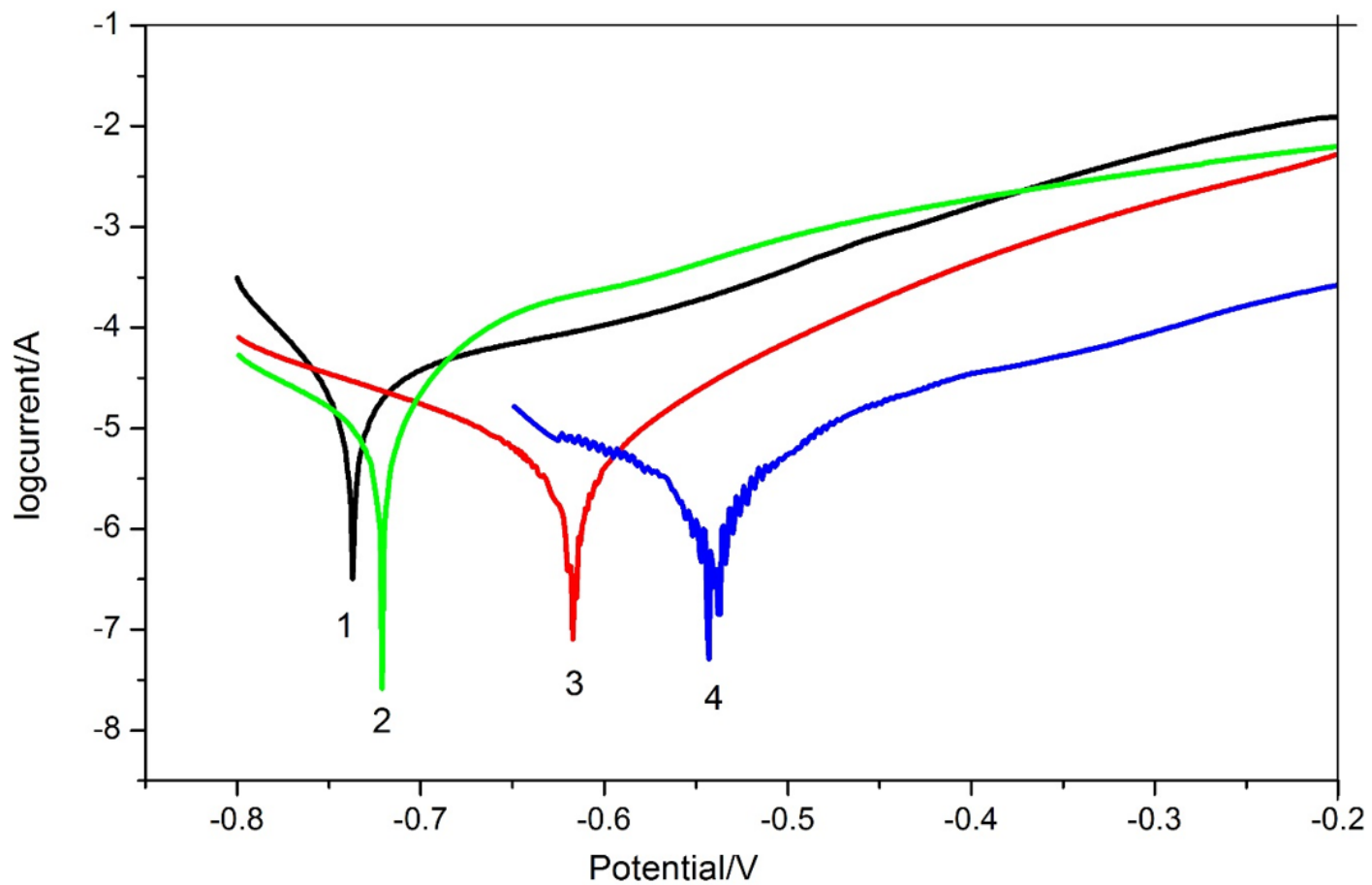


Fig 10.

Figure 10

Anodic polarization curves of 1) bare MS 2)PIn3/MS, 3)PIn2/MS and 4)PIn1/MSin % 3.5w.t NaCl at room temperature.

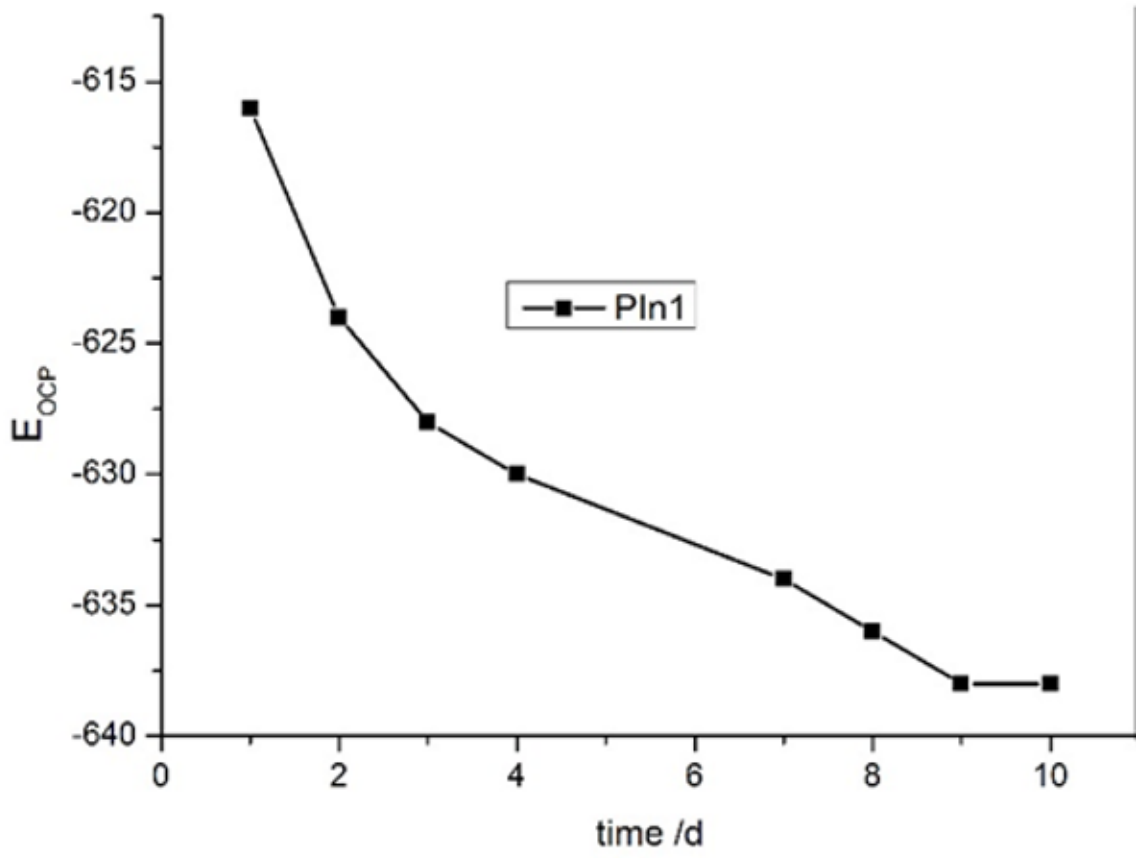


Fig. 11

Figure 11

Eocp-time diagram of PIn1

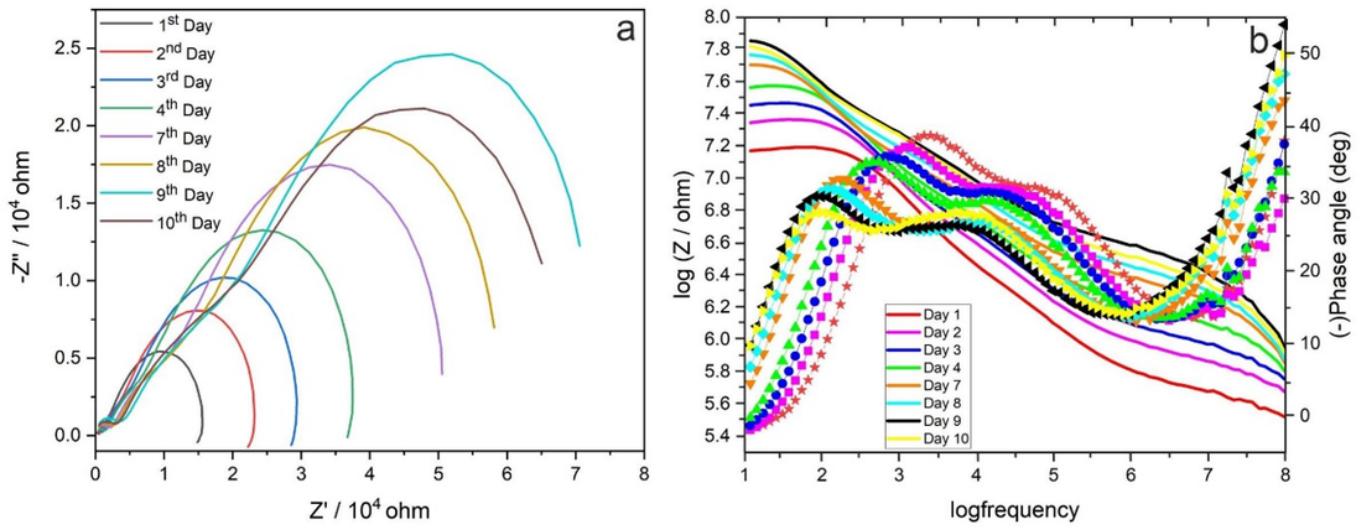


Fig 12

Figure 12

a) Nyquist plot b) Bode and phase angel-logfrequency plots of Pln1 immersed at 20 °C for different days (1, 2, 3, 4, 7,8 ,9, and 10 days)

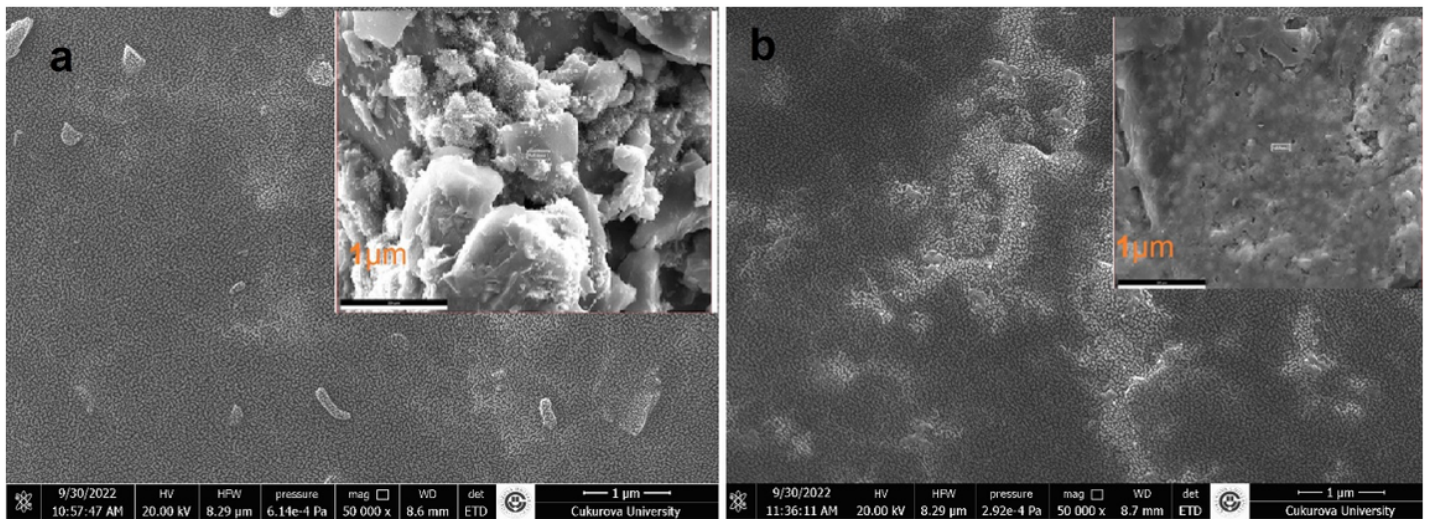


Fig. 13.

Figure 13

SEM images of Pln1 a) before b) after long term corrosion tests at different magnifications

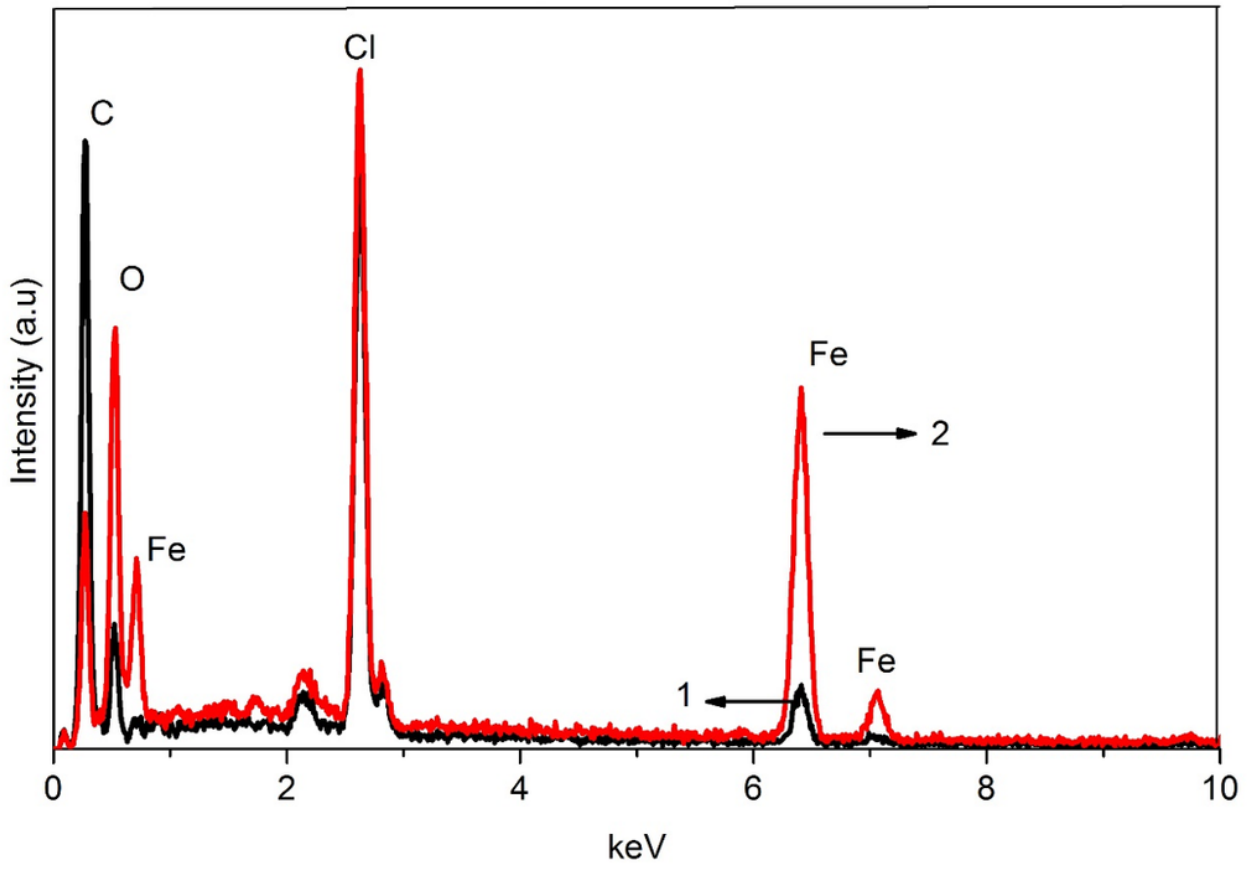


Fig 14.

Figure 14

EDX diagram of Pln1 1) before 2) after long term corrosion tests

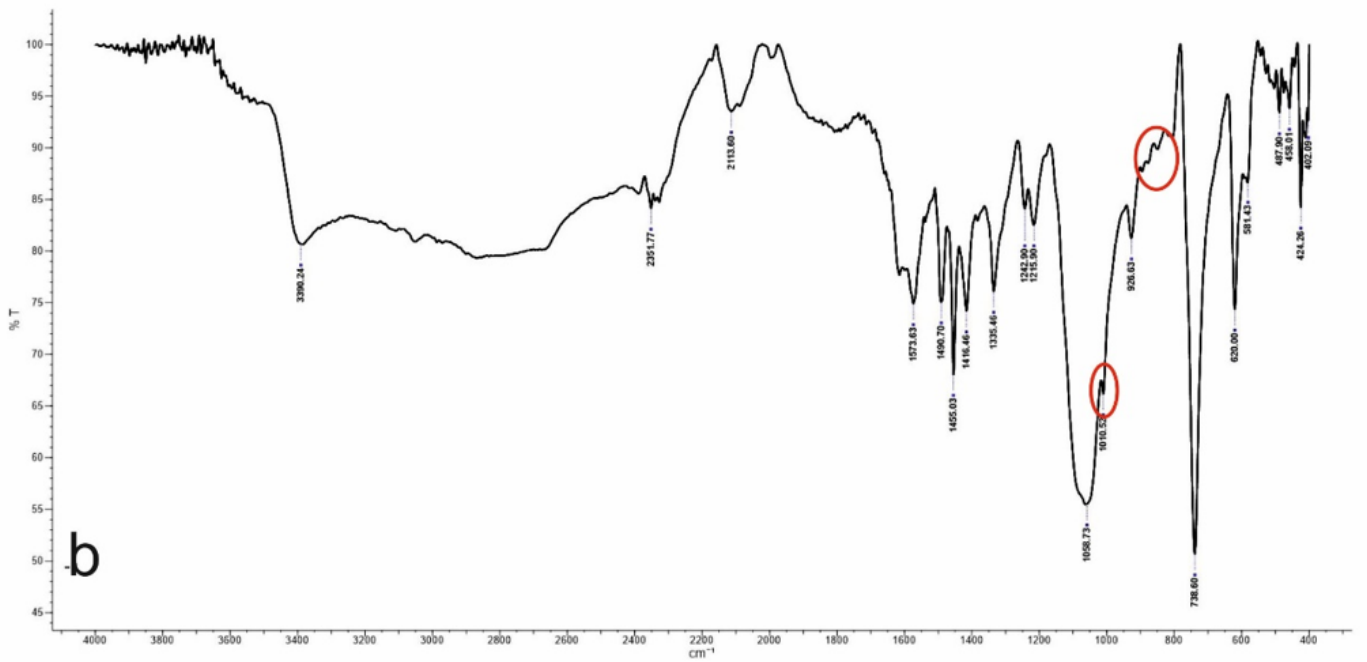
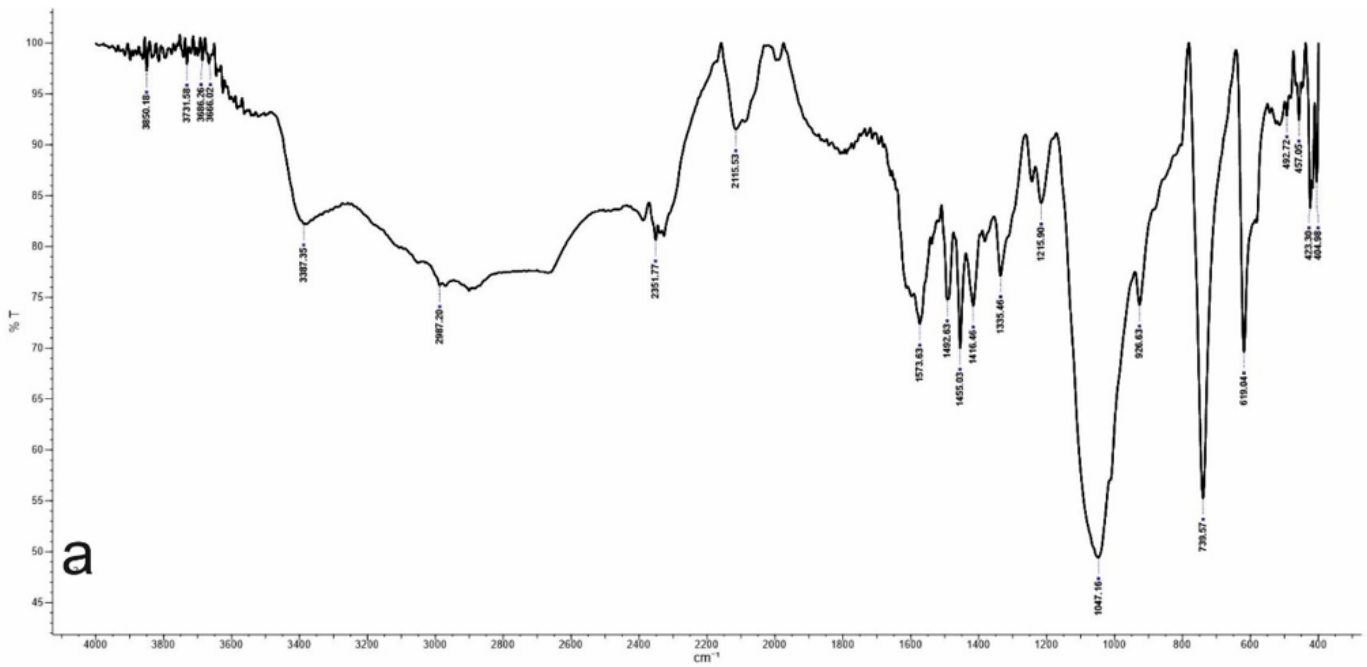


Fig 15.

Figure 15

FTIR spectrum of Pln1 a) before b) after long term corrosion testes

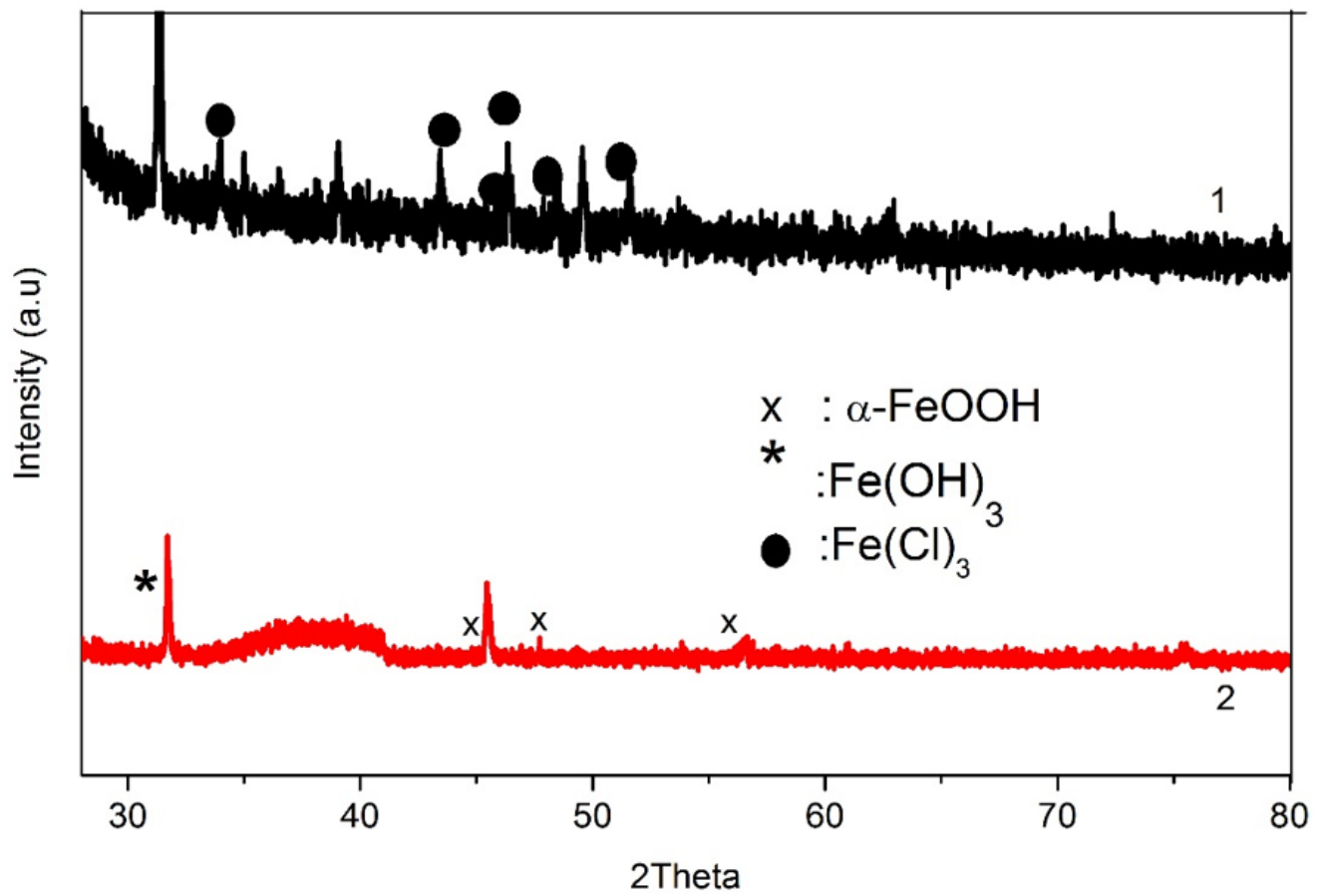


Fig 16.

Figure 16

XRD pattern of Pln1 1) before and, 2) after long term corrosion tests

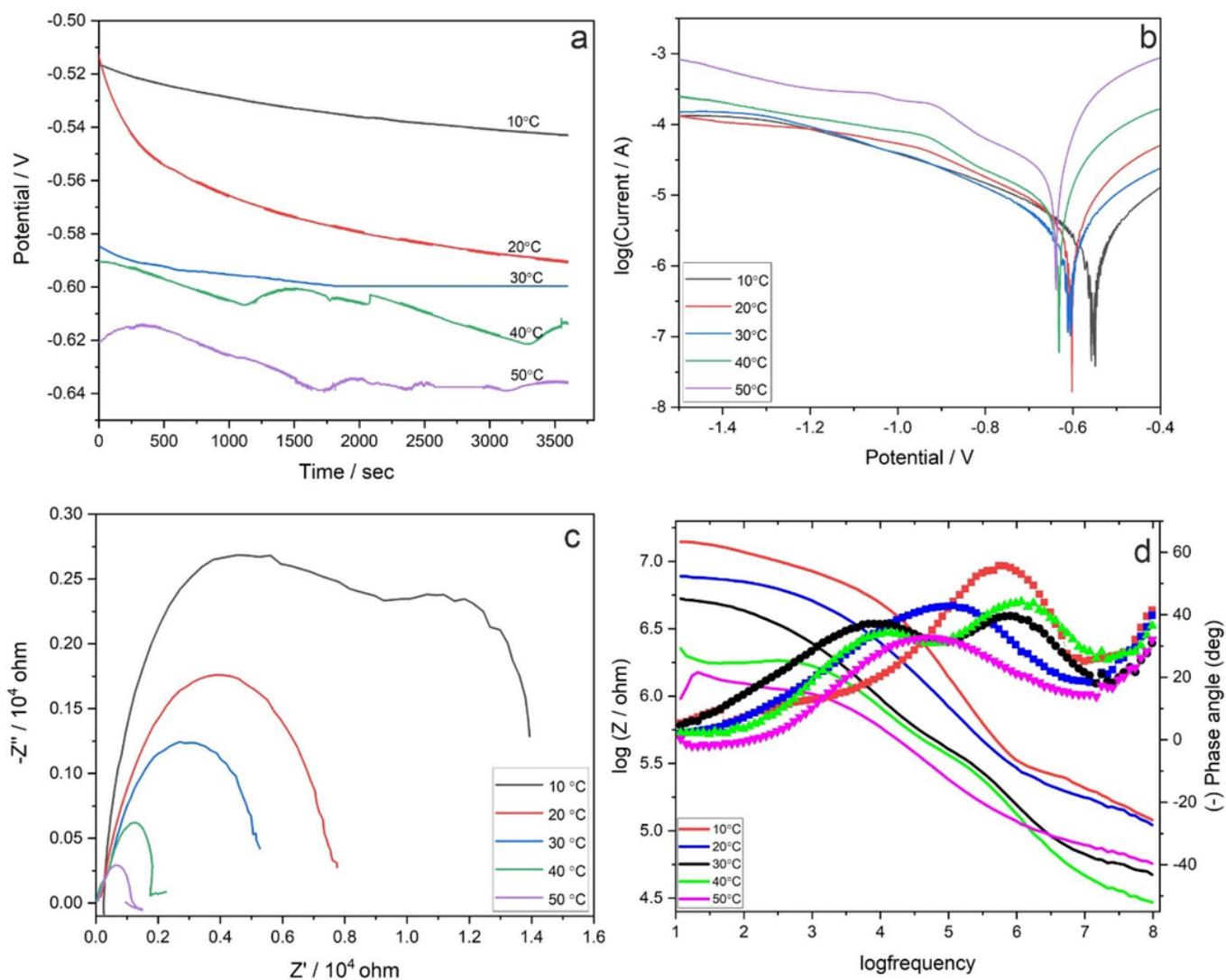


Fig 17.

Figure 17

a) E_{ocp} -t diagram of PIn1 b) Cathodic polarization curves of PIn1 in 3.5 % NaCl at different temperatures (10, 20, 30, 40, and 50 °C) c) Nyquist plot d) Bode and phase angle plots of PIn1 immersed in 3.5% NaCl at 10, 20, 30, 40, and, 50 °C.